

# Water Resources Research



## **RESEARCH ARTICLE**

10.1029/2022WR032329

#### **Key Points:**

- Two-station monitoring disentangles nitrate uptake pathways and their temporal dynamics in heterogeneous high-order streams
- Net nitrate uptake exhibits high variation, seasonally and across reach conditions, with cases of consistent net release
- Heterotrophic nitrate uptake and release were higher during post-wet seasons and exhibited various diel patterns

#### **Supporting Information:**

Supporting Information may be found in the online version of this article.

#### Correspondence to:

X. Yang, xiaoqiang.yang@ufz.de

#### Citation:

Zhang, X., Yang, X., Hensley, R., Lorke, A., & Rode, M. (2023). Disentangling in-stream nitrate uptake pathways based on two-station high-frequency monitoring in high-order streams. *Water Resources Research*, 59, e2022WR032329. https://doi.org/10.1029/2022WR032329

Received 9 MAR 2022 Accepted 13 FEB 2023

## **Author Contributions:**

Xiaoqiang Yang

Formal analysis: Xiaolin Zhang.

Methodology: Xiaolin Zhang, Robert Hensley, Michael Rode Supervision: Xiaoqiang Yang, Andreas Lorke, Michael Rode Writing – original draft: Xiaolin Zhang Writing – review & editing: Xiaoqiang Yang, Robert Hensley, Andreas Lorke, Michael Rode

© 2023. The Authors.

This is an open access article under the terms of the Creative Commons Attribution License, which permits use, distribution and reproduction in any medium, provided the original work is properly cited.

# Disentangling In-Stream Nitrate Uptake Pathways Based on Two-Station High-Frequency Monitoring in High-Order Streams

Xiaolin Zhang<sup>1</sup>, Xiaoqiang Yang<sup>1,2</sup>, Robert Hensley<sup>3</sup>, Andreas Lorke<sup>4</sup>, and Michael Rode<sup>1,5</sup>, Department of Aquatic Ecosystem Analysis and Management, Helmholtz Centre for Environmental Research - UFZ, Magdeburg, Germany, Department of Ecohydrology and Biogeochemistry, Leibniz Institute of Freshwater Ecology and Inland Fisheries (IGB), Berlin, Germany, Battelle - National Ecological Observatory, Network, Boulder, CO, USA, Anstitute

Magdeburg, Germany, <sup>2</sup>Department of Ecohydrology and Biogeochemistry, Leibniz Institute of Freshwater Ecology and Inland Fisheries (IGB), Berlin, Germany, <sup>3</sup>Battelle - National Ecological Observatory Network, Boulder, CO, USA, <sup>4</sup>Institute for Environmental Sciences, University of Koblenz-Landau, Landau, Germany, <sup>5</sup>Institute of Environmental Science and Geography, University of Potsdam, Potsdam, Germany

**Abstract** In-stream nitrate (NO<sub>3</sub><sup>-</sup>) uptake in rivers involves complex autotrophic and heterotrophic pathways, which often vary spatiotemporally due to biotic and abiotic drivers. High-frequency monitoring of NO<sub>3</sub> mass balance between upstream and downstream measurement sites can quantitatively disentangle multipath NO<sub>3</sub><sup>-</sup> uptake dynamics at the reach scale. However, this approach remains limited to a few river types and has not been fully explored for higher-order streams with varying hydro-morphological and biogeochemical conditions. We conducted two-station 15-min monitoring in five high-order stream reaches in central Germany, calculating the NO<sub>3</sub>--N mass balance and whole-stream metabolism based on time series of NO<sub>3</sub>--N and dissolved oxygen, respectively. With thorough considerations of lateral inputs, the calculated net NO<sub>3</sub><sup>-</sup>-N uptake rates ( $U_{\rm NET}$ ) differed substantially among campaigns (ranging from -151.1 to 357.6 mg N m<sup>2</sup> d<sup>-1</sup>, with cases of negative values representing net  $NO_3^-$ -N release), and exhibited higher  $U_{NET}$  during the post-wet season than during the dry season. Subtracting autotrophic assimilation ( $U_A$ , stoichiometrically coupled to stream metabolism) from  $U_{\text{NET}}$ ,  $U_D$  represented the net balance of heterotrophic NO<sub>3</sub><sup>-</sup>-N uptake ( $U_D > 0$ , the dominance of denitrification and heterotrophic assimilation) and  $NO_3^-$ -N release ( $U_D < 0$ , the dominance of nitrification/mineralization). This rarely reported uptake pathway contributed substantially to  $U_{\rm NET}$  patterns, especially during post-wet seasons; moreover, it appeared to exhibit various diel patterns, and for  $U_D > 0$ , diel minima occurred during the daytime. These findings advance our understanding of complex reach-scale N-retention processes and can help develop future modeling concepts at the river-network scale.

## 1. Introduction

Excessive anthropogenic nitrogen (N) runoff from watersheds has been increasingly polluting aquatic ecosystems and causing eutrophication problems (Smith, 2003; Smith et al., 1999). One of the major diffuse sources is the intensive application of fertilizers to increase agricultural production. This anthropogenic N (mainly nitrate-nitrogen ( $NO_3^--N$ )) has elevated  $NO_3^-$  levels in river networks (Billen et al., 2013; Fowler et al., 2013). The capacity of stream biota to take up  $NO_3^-$  from the water column has attracted the attention of environmental scientists and managers in the past few decades. Specifically, in-stream  $NO_3^-$  retention processes across headwater streams and higher-order rivers have been found to buffer and mitigate significant  $NO_3^-$  transport to downstream waterbodies (Alexander et al., 2000; Zhao et al., 2015).

Despite this critical importance, accurately estimating rates of in-stream  $NO_3^-$  uptake at reach scales remains difficult, and partitioning it among different pathways (e.g., assimilation, denitrification) is even more difficult. Assimilation by photoautotrophs ( $U_A$ ) is closely correlated with stream metabolism and, therefore, can be informed by gross primary production - GPP (Heffernan et al., 2010; Jarvie et al., 2018; Lupon et al., 2016). Heterotrophic uptake consists of assimilative uptake by heterotrophic microorganisms and dissimilatory denitrification (Jarvie et al., 2018). These various uptake pathways are influenced by both biotic and abiotic characteristics of the stream (Alberts et al., 2017; Heffernan et al., 2010; Kunz et al., 2017). The complex convolution of these drivers at the reach scale could result in high spatial and temporal variations in overall in-stream  $NO_3^-$  dynamics. The seasonality of incoming solar radiation and shading by riparian vegetation can strongly influence GPP-related  $U_A$  (Alberts et al., 2017; Lupon et al., 2016; Yang et al., 2019).  $NO_3^-$  uptake processes can also be strongly impacted by the seasonal variations of water temperature and flow conditions (Chamberlin et al., 2021;

ZHANG ET AL. 1 of 17

Hensley et al., 2015). Spatially, agricultural and urban streams often exhibit high  $U_A$  due to less riparian shading (in addition to elevated nutrient levels), their net  $NO_3^-$  uptake is often much lower than in forested streams where heterotrophic uptake rates can be much higher (Arango et al., 2008). Restoring forest riparian buffers in these human-altered streams has been suggested as a best management practice to help re-establish natural ranges of in-stream  $NO_3^-$  processing (Sobota et al., 2012; Sweeney et al., 2004). Finally, channel modifications are another important factor that influences denitrification efficiency by affecting the water exchange with hyporheic zones (Gomez-Velez et al., 2015).

Several methods have been used to quantify NO<sub>3</sub><sup>-</sup> uptake and partition it into constituent pathways. Each has inherent advantages and disadvantages. One approach is to add <sup>15</sup>N (Hall et al., 2009; Mulholland et al., 2002). While this can provide pathway-specific inferences (Mulholland et al., 2009; Tank et al., 2018), its reliance on costly isotope addition logistically restricts its application to smaller streams. Pulse injections of unlabeled nutrients are an alternative approach (Covino et al., 2010) that can also be applied to larger rivers (Tank et al., 2018), but usually provides no pathway-specific inferences. Moreover, these tracer-addition methods only capture a snapshot representing a single set of conditions without considering temporal dynamics. More recently, advances in high-frequency in-situ sensor technology have enabled continuous high-frequency monitoring of in-stream water quality parameters (Burns et al., 2019; Pellerin et al., 2012; Rode, Wade, et al., 2016). Because approaches based on in-situ monitoring are passive, they can be applied across stream orders and over extended periods of time, and their high temporal resolution can help explore variation in NO<sub>3</sub><sup>-</sup> uptake at sub-daily scales (Chamberlin et al., 2021; Rode, Halbedel Née Angelstein et al., 2016).

Despite this advantage, several challenges remain, particularly regarding the disentangling of processing pathways. Heffernan and Cohen (2010) quantified NO<sub>3</sub><sup>-</sup> assimilation and the sum of denitrification and heterotrophic assimilation based on diel variations in NO<sub>3</sub><sup>-</sup> concentrations in a spring-fed river (i.e., constant inputs) at a single sampling station. Dissolved oxygen (DO), commonly used to estimate GPP using a single station, continuously re-equilibrates with the atmosphere and limits the distance over which upstream inputs affect the downstream signal (Hensley & Cohen, 2016). This is not the case for the non-gaseous solute NO<sub>3</sub><sup>-</sup>, and so the use of the one-station method is often restricted to a limited range of hydrological conditions (Rode, Halbedel Née Angelstein et al., 2016; Yang et al., 2019). Alternatively, approaches based on two stations relax these constraints and have been successfully applied to investigate in-stream processes related to non-gaseous solutes such as NO<sub>3</sub><sup>-</sup> (Hensley & Cohen, 2016; Kunz et al., 2017). Moreover, combining measurements of stream metabolism and NO<sub>3</sub><sup>-</sup> mass balance can help disentangle and partition uptake pathways (Jarvie et al., 2018). In particular, this approach allows for subtracting assimilation uptake  $(U_A)$  from net uptake  $(U_{NET})$  to quantify the rarely investigated remaining part  $(U_D)$ , which represents heterotrophic uptake or  $NO_3^-$  release (Jarvie et al., 2018). Yet, the potential of multi-parameter two-station approaches has not been fully explored for describing dynamics of NO<sub>3</sub><sup>-</sup> uptake patterns in high-order reach with different stream conditions and during different seasons, nor for investigating detailed sub-daily patterns of pathway-specific NO<sub>3</sub><sup>-</sup> uptake processes.

Here, we performed 11 campaigns of two-station, high-frequency, multi-parameter monitoring in five stream reaches in central Germany, which exhibit a variety of stream conditions in terms of morphological sinuosity, riparian, and surrounding vegetation conditions. The objectives of this study were (a) to apply multi-parameter two-station approaches to disentangle  $NO_3^-$  uptake pathways (i.e., the net uptake  $U_{NET}$ , autotrophic assimilation  $U_A$  and their differences inferred heterotrophic uptake  $U_D$ ) in heterogeneous high-order stream reaches under low-flow conditions, (b) to investigate pathway-specific uptake patterns and their variations between late spring (post-wet season) and summer (dry season) with varying stream conditions, and (c) to analyze the sub-daily pattern of  $U_D$  and its variability under different stream and seasonal conditions.

## 2. Data and Methods

## 2.1. Study Reaches

We selected two reaches (ca. 6 km each) in the fourth-order middle Weiβe Elster River and three reaches (ranged 3–7 km) in the sixth-order middle and lower Bode River, all located in the lowland region of central Germany (Figure 1). These reaches exhibited substantial variations in stream morphological and surrounding landuse conditions (Table 1). The Weiβe Elster River, ca. 250 km long, originates in the border region between the Czech Republic and Germany and flows north into the Saale River, Germany. In the middle Weiβe Elster

ZHANG ET AL. 2 of 17

1944/1973, 2023, 3, Downloaded from https://agupubs.onlinelibrary.wiley.com/doi/10.1029/2022WR032329, Wiley Online Library on [16/03/2023]. See the Terms and Conditions (https://online

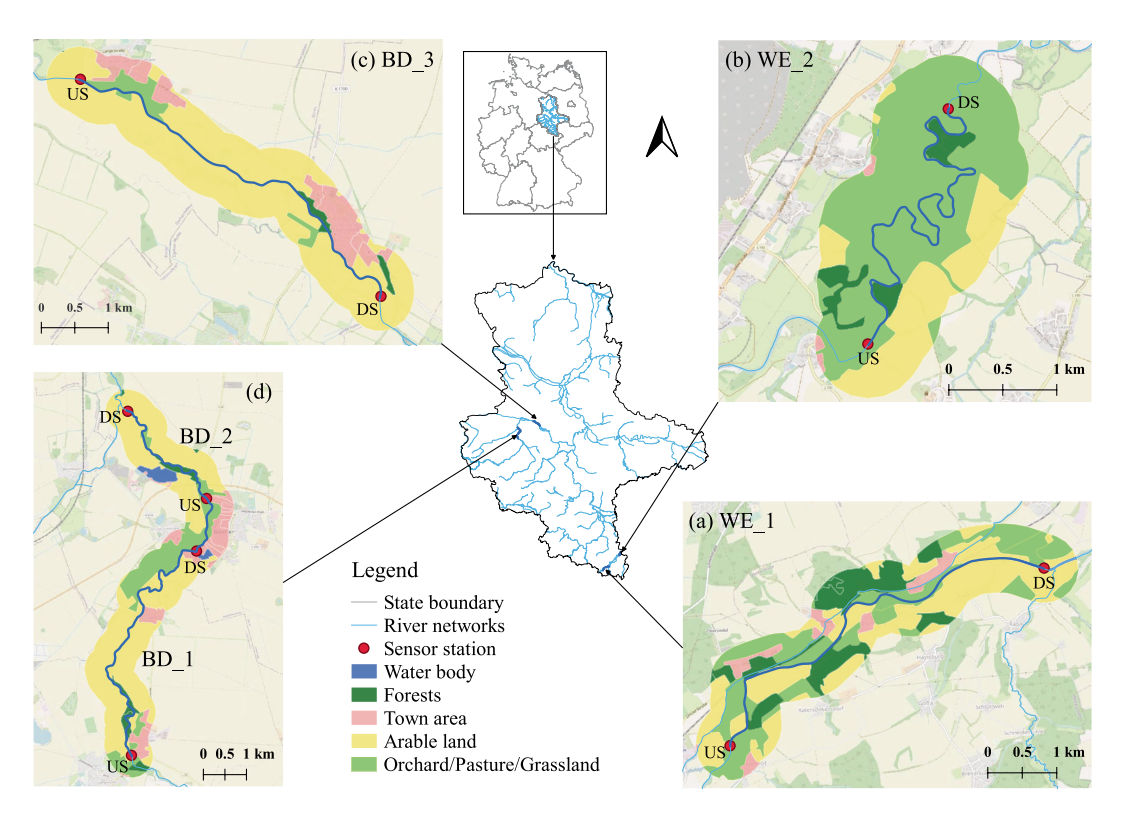


**Figure 1.** Locations of the five monitored stream reaches in Saxony-Anhalt, Germany, showing the two-station monitoring design (upstream station (US) and downstream station (DS)) and the riparian and morphological conditions of the reaches. The background map was taken from OpenStreetMap and riparian land uses (500 m on each side of the reaches) from CORINE (2018).

where the study reaches are located, NO<sub>3</sub><sup>-</sup>-N concentrations have been increasing due to intensive agricultural activities and effluent release from sewage-treatment plants (Wagenschein & Rode, 2008). The upstream reach (WE\_1) (Figure 1a) and downstream reach (WE\_2) (Figure 1b) have contrasting hydromorphological conditions (Table 1): WE\_1 is artificially channelized and surrounded by arable land, whereas WE\_2 conserves a highly sinuous morphology and passes through a patch of agricultural grassland. We stopped reaching WE\_2 ca. 100 m upstream of the mining drainage to avoid the influence of groundwater discharge from the mine (Kunz et al., 2017). The groundwater table in this area is low due to mining, which restricted interactions with groundwater during our measurements. Riparian deciduous trees surround the river corridor of both reaches, and the stream is partly shaded by broad leaves during the vegetation season.

The Bode River, ca. 169 km long, originates in the Harz Mountain area and flows into the Saale River. The middle and lower parts of the Bode watershed have long been used for intensive agriculture, due to highly fertile Chernozem soils (Wollschläger et al., 2017). We chose two reaches (BD\_1 and BD\_2) in the middle Bode upstream of the confluence with the major tributary, the Holtemme, which is impacted by urban effluent. Both reaches have relatively little sinuosity, indicating significant channel modification for surrounding agricultural use. Compared to BD\_1 and BD\_2, the lower Bode reach (BD\_3) has a straighter river corridor (classified as "completely changed" by the State Agency for Flood Protection and Water Management of Saxony-Anhalt, Germany (LHW, 2022)) and is wider, with a gentler slope (Figures 1c and Table 1). In addition, more macrophytes were observed in BD\_3 than in BD\_1 and BD\_2. Riparian vegetation, including deciduous trees, is extensive in all reaches, in addition to the varying surrounding land uses (Figure 1). The hydrology of the Bode River corridor has been altered by engineering structures. One weir is located between BD\_1 and BD\_2 and another is located ca. 700 m downstream of the BD\_3 downstream stations, both of which alter stream hydraulic characteristics and impound water upstream of the weirs.

Discharge measurements were obtained from the nearest gauging stations operated by LHW: the Zeitz station (51°03'26"N, 12°08'37"E) for the Weiβe Elster, the Wegeleben station (51°53'15"N, 11°11'22"E) for the middle

ZHANG ET AL. 3 of 17



**Table 1** *Morphological Features of River Reaches and Overview of Monitoring Deployments* 

Reach	River	Length (m)	Width (m)	Sinuosity	Slope (‰)	River morphology status <sup>a</sup> and surrounding landscape <sup>b</sup>	Deployment periods (start date-end date)	Campaigns (seasons)
WE_1	Weiße Elster	6,280	23	1.20	0.5	Strongly modified and straightened; intensive arable land	2019/05/13–2019/05/16	2019-05 WE_1 (post-wet)
							2019/09/18–2019/09/23	2019-09 WE_1 (dry)
WE_2	Weiße Elster	6,100	23	2.65	0.89	Slightly modified and remains meandering; permanent grassland	2019/05/16–2019/05/20	2019-05 WE_2 (post-wet)
							2019/09/23–2019/09/26	2019-09 WE_2 (dry)
BD_1	Middle Bode	7,170	17	1.44	0.6	Slightly modified; considerable riparian forest and grassland	2019/06/17–2019/06/20	2019-06 BD_1 (post-wet)
							2020/08/03-2020/08/10	2020-08 BD_1 (dry)
BD_2	Middle Bode	3,360	17	1.24	0.6	Slightly to moderately modified; arable land with some forest	2019/06/20–2019/06/24	2019-06 BD_2 (post-wet)
							2020/08/12-2020/08/19	2020-08 BD_2 (dry)
							2021/07/19–2021/08/02	2021-07 BD_2 (transition)
BD_3	Lower Bode	6,150	20	1.12	0.036	Completely changed; intensive arable land	2019/08/21–2019/08/26	2019-08 BD_3 (dry)
							2020/08/27-2020/09/03	2020-08 BD_3 (dry)

*Note.* Sinuosity: the ratio of the curvilinear length (along the reach) to the Euclidean distance (straight line) between the end points of the reach. 
<sup>a</sup>based on the "watercourse development status" classification of LHW (2022). 
<sup>b</sup>CORINE (2018) from BKG.

Bode and the Hadmersleben station ( $52^{\circ}00'20^{\circ}N$ ,  $11^{\circ}19'09''E$ ) for the lower Bode, for which mean discharge from 2016 to 2020 was 11.99, 5.11, and 8.04 m<sup>3</sup> s<sup>-1</sup>, respectively. All campaigns were conducted during the low-flow period (May-September, see annual hydrographs in Figure S1 in Supporting Information S1). Flow velocity ranged from 0.25 to 0.40 and 0.10–0.30 m s<sup>-1</sup> in the WE and BD reaches, respectively, estimated specifically for each campaign using the specific conductivity informed travel times (see Method 2.2).

#### 2.2. Sensor Deployment and Data Collection

For each reach selected, we set up in-situ sensors to monitor water chemistry at the upstream and downstream stations. At each station, an automated ultraviolet spectrophotometer (OPUS, ProPS WW, TriOS, Germany) was deployed to measure  $NO_3^{-}$ -N concentration, with a precision of 0.03 mg  $L^{-1}$  and accuracy of  $\pm 2\%$ . We used a sensor path length of 10 mm to measure absorption at wavelengths of 190–360 nm. Before each deployment, the sensors were calibrated and checked for measurement offsets by pre-running them side by side in the same stream water. A multi-parameter water-quality probe (EXO², YSI Environment, USA) was deployed to simultaneously measure water temperature (precision 0.001°C, accuracy  $\pm$  0.01°C), turbidity (precision 0.01 FNU, accuracy  $\pm$  2% FNU), pH (precision 0.01 units, accuracy  $\pm$  0.1), specific conductivity (precision 0.1  $\mu$ S cm<sup>-1</sup>, accuracy  $\pm$  0.5%), dissolved oxygen (DO, precision 0.01 mg  $L^{-1}$ , accuracy  $\pm$  1%) and *chlorophyll a* (*Chl-a*, precision 0.01  $\mu$ g  $L^{-1}$ , linearity:  $R^2 > 0.999$  for serial dilution of Rhodamine WT solution from 0 to 400  $\mu$ g  $L^{-1}$ ). The two sensors were installed in a 20 cm diameter vented pipe to protect them from debris and other disturbances. The measurement frequency of both sensors was set to 15 min.

We conducted two or three campaigns per reach in different seasons (either from May-June or August-September, representing post-wet and dry seasons, respectively). One additional campaign was conducted at BD\_2 in July 2021, representing the transitional season (Table 1; Figure S1 in Supporting Information S1). The deployment durations varied between 3 and 14 days. The sensor built-in automatic cleaning wipers operated every 1 hr to

ZHANG ET AL. 4 of 17

prevent biofilm accumulation. During the 14-day campaign (2021-07 BD\_2), we manually cleaned the pipes and probes at both stations after 7 days to ensure the data quality. We manually sampled water at both upstream and downstream stations on the first and last day of each campaign. Samples were prepared following the standard procedures in the Central Laboratory for Water Analytics & Chemometrics, Helmholtz Center for Environmental Research – UFZ, Magdeburg, Germany. Detailed analytical descriptions can be found in Friese et al. (2014). NO<sub>3</sub><sup>-</sup>-N , nitrite-N (NO<sub>2</sub><sup>-</sup>-N), ammonium-N (NH<sub>4</sub><sup>+</sup>-N), total N (TN), soluble reactive phosphorus (SRP), and total phosphorus (TP) concentrations were measured. Concentrations of NH<sub>4</sub><sup>+</sup>-N were always low (with mean value 0.053 mg L<sup>-1</sup>) in our study regions, therefore, we exclusively focused on NO<sub>3</sub><sup>-</sup>-N uptake (Table S2 in Supporting Information S1). The laboratory analyses of grab sample NO<sub>3</sub><sup>-</sup>-N concentrations were used as benchmarks for sensor verification, as instructed in the sensor manual. Finally, we performed longitudinal profiling (similar to Kunz et al., 2017) during the first campaign in each reach to identify potential inflows, for example, small ditches and sewage pipes along the reach. During each of these longitudinal profiles, we measured the same water chemistry parameters as we did at each upstream and downstream station.

Sub-daily variation in specific conductivity was used as a natural tracer to estimate the mean travel time ( $\tau$ ) from upstream to downstream stations during each campaign by calculating the mean time lag between each corresponding peak and valley (for detailed information, see Text S1 in Supporting Information S1). Similar variations in NO<sub>3</sub><sup>-</sup>-N concentrations were then used to cross-validate  $\tau$  to ensure that it was estimated reasonably well.

## 2.3. Two-Station Method for Assessing Net Nitrate Uptake and Stream Metabolism

The two-station method was used to calculate reach-scale net  $NO_3^-$ -N uptake and stream metabolism. The areal net  $NO_3^-$ -N uptake ( $U_{NET}$ ) was calculated as the difference between inputs (from the upstream  $NO_3^-$ -N flux  $Q_{US,t-\tau/2} \times \left[NO_3^- - N\right]_{US,t-\tau/2}$  and lateral seepage flux  $Q_{L,t} \times \left[NO_3^- - N\right]_{L,t}$ ) and outputs (downstream flux  $Q_{DS,t+\tau/2} \times \left[NO_3^- - N\right]_{DS,t+\tau/2}$ ), divided by total benthic area ( $w \times L$ ):

$$U_{NET,t} = \frac{Q_{US,t-\frac{\tau}{2}} \times \left[NO_3^- - N\right]_{US,t-\frac{\tau}{2}} + Q_{L,t} \times \left[NO_3^- - N\right]_{L,t} - Q_{DS,t+\frac{\tau}{2}} \times \left[NO_3^- - N\right]_{DS,t+\frac{\tau}{2}}}{w \times L} \tag{1}$$

where  $Q_{US}$  and  $Q_{DS}$  denote upstream and downstream discharge, respectively (here we used the same values from nearby discharge gauging stations, Section 2.1); the width (w) was taken as the average between upstream and downstream stations. Note that time-series of upstream and downstream fluxes were adjusted by  $-\tau/2$  and  $+\tau/2$ , respectively, based on the estimated travel time  $\tau$  between the two stations. Positive  $U_{NET,t}$  indicates net  $NO_3^-$ -N uptake, whereas negative  $U_{NET,t}$  indicates net  $NO_3^-$ -N release.

The lateral discharge inputs ( $Q_L$ ) of three Bode reaches were estimated based on the drainage areas between the upstream and downstream stations and the daily runoff depth simulated using a grid-base catchment hydrological model. The NO<sub>3</sub><sup>-</sup>-N concentration of the lateral inputs was assigned as 2 mg L<sup>-1</sup> for BD\_1 and BD\_2, 6.75 mg L<sup>-1</sup> for BD\_3 according to measurements from Bode lowland tributaries (from the state water authority-LHW). For the Weiße Elster reaches, we did not consider lateral inputs because of the small sub-areas and low groundwater levels. Further details of these lateral input considerations are provided in Supplementary Text S3 in Supporting Information S1.

Stream metabolism is typically measured using a one-station approach (Odum, 1956), but this method integrates over the entire upstream length required for reaeration to attenuate a diel signal (Chapra & Di Toro, 1991; Hensley & Cohen, 2016). This length ( $\sim 3*v/k$ ) is much longer than that of our study reaches (Table S3 in Supporting Information S1). To estimate metabolism occurring within the same reach area as  $U_{NET}$ , we estimated areal net ecosystem production (NEP) using a two-station method. NEP was calculated from the mass-balance equation, which included measured DO concentrations and a reaeration term based on the Demars et al. (2011) method:

$$NEP_{t} = \frac{Q_{DS,t+} \frac{\tau}{2} [DO]_{DS,t+} \frac{\tau}{2} - Q_{US,t-} \frac{\tau}{2} [DO]_{US,t-} \frac{\tau}{2} - kQ_{t} [DO]_{def,t}}{w \times L}$$
(2)

where k denotes the reaeration coefficient that is determined by the energy dissipation model (Tsivoglou & Neal, 1976) considering impacts of discharge and slope.  $[DO]_{def}$  denotes the difference between saturation DO

ZHANG ET AL. 5 of 17

9447973, 2023, 3, Downloaded from https

Overview of High-Frequency Measurements and Stream Characteristics for the 11 Campaigns (i.e., Means of Upstream and Downstream Measurements)  WE_1  WE_2  BD_1  BD_1  BD_2  BD_2  BD_3  B			$BD_3$	30 0000
of High-Frequency Measurements and Stream Characteristic  WE_1  WE_1  O010 05				70 100
of High-Frequency Measurements and Stream Characteristic  WE_1  WE_1  O010 05		n Measurements)	BD_2	80 0000
of High-Frequency Measurements and Stream Characteristic  WE_1  WE_0		n and Downstrean		20.010.06
of High-Frequency Measurements and Stream Characteristic  WE_1  WE_0		eans of Upstrean	)_1	80 0000
of High-Frequency Measurements and Stream Characteristic  WE_1  WE_0		npaigns (i.e., Ma	BI	20.0100
of High-Frequency Measurements and Strear  WE_1		ics for the 11 Car	3_2	2010 00
of High-Frequency Measur		am Characteristi	WE	20.0100
of High-Frequency Mee		ırements and Stre	E_1	00 0100
Table 2  Overview of High-		Frequency Measu	[W	20.010
	Table 7	Overview of High-		Domonoton

	W	$WE_{-}1$	WE_2	2	BD	2_1		BD_2		BD_3	£_3
Parameter	2019–05	2019–09	2019–05	2019–09	2019–06	2020-08	2019–06	2020-08	2021–07	2019–08	2020-08
$Q(m^3 s^{-1})$	$9.06 \pm 0.38$	$4.55 \pm 0.18$	$8.58 \pm 0.44$	$4.75 \pm 0.26$	$2.5 \pm 0.11$	$1.57 \pm 0.08$	$2.34 \pm 0.17$	$1.65 \pm 0.31$	$1.93 \pm 0.17$	$1.98 \pm 0.11$	$2.2 \pm 0.06$
T (°C)	$11.84 \pm 0.97$	$13.09 \pm 0.5$	$13.29 \pm 2.1$	$15.17 \pm 0.41$	$19.52 \pm 0.7$	$19.3 \pm 1.39$	$19.35 \pm 0.47$	$20.65 \pm 0.64$	$18.54 \pm 1.11$	$18.56 \pm 0.78$	$16.74 \pm 0.24$
$N \text{ (mg L}^{-1})$	$3.84 \pm 0.05$	$3.85\pm0.13$	$3.62 \pm 0.11$	$3.51 \pm 0.05$	$1.76\pm0.03$	$1.23 \pm 0.05$	$1.65\pm0.05$	$1.22 \pm 0.08$	$1.73 \pm 0.09$	$1.23 \pm 0.06$	$1.01 \pm 0.06$
$DO \; (mg \; L^{-1})$	$10.86 \pm 0.54$	$10.33 \pm 0.3$	$10.84 \pm 0.82$	$9.99 \pm 0.73$	$8.68 \pm 0.45$	$8.59 \pm 0.37$	$8.77 \pm 0.35$	$8.16\pm0.37$	$8.82 \pm 0.41$	$9.32 \pm 1.18$	$9.45 \pm 0.54$
Turb (FNU)	$1.91 \pm 0.23$	$1.53 \pm 0.16$	$1.78\pm0.11$	$1.52\pm0.17$	$3.84 \pm 0.17$	$1.8\pm0.22$	$4.21 \pm 0.44$	$2.11 \pm 0.58$	$4.05 \pm 0.61$	$1.2 \pm 0.14$	$1.2\pm0.11$
Hq	$8.13 \pm 0.08$	$8.44 \pm 0.05$	$8.26\pm0.1$	$8.65 \pm 0.06$	$8.25\pm0.07$	$7.97 \pm 0.04$	$8.23 \pm 0.05$	$7.88 \pm 0.05$	$8.01 \pm 0.05$	$8.15\pm0.11$	$8.03 \pm 0.06$
SpCond ( $\mu S \text{ cm}^{-1}$ )	$850.5 \pm 52.5$	$850.5 \pm 52.5  1224.4 \pm 39.0$	$1051.9 \pm 32.1$	$1337.6 \pm 16.1$	$727.5 \pm 6.5$	$733.0 \pm 23.5$	$822.6 \pm 21.6$	$789.0 \pm 48.6$	$768.6 \pm 32.9$	$1094.1 \pm 12.5$	$1169.9 \pm 31.6$
$Chl-a~(\mu g~L^{-1})$	$4.19\pm0.57$	$2.72 \pm 0.47$	$2.63 \pm 0.45$	$3.2 \pm 0.26$	$2.12\pm0.15$	$2.84 \pm 0.58$	$2.19 \pm 0.13$	$2.8 \pm 0.6$	$1.35\pm0.13$	$4.46 \pm 0.85$	$2.57 \pm 0.13$
τ (h)	S	7	4.5	9	∞	14	3.5	4.5	4	14	15.5
$v \text{ (m s}^{-1})$	0.35	0.25	0.38	0.28	0.25	0.14	0.27	0.21	0.23	0.12	0.11
$k (10^{-5} \text{ s}^{-1})$	3.84	3.85	3.62	3.51	1.76	1.23	1.65	1.22	1.73	1.23	1.01
Note. Q: discharge. T: water temperature. N: NO <sub>3</sub> N concentration. DO: dissolved oxygen. Turb: turbidity. SpCond: specific conductivity. Chl-a: chlorophyll a. τ: travel time from upstream to downstream stations. υ: velocity. calculated by dividing river length by τ.	. T: water tempers. v: velocity. ca	erature. N: NO <sub>3</sub>	-N concentration.	DO: dissolved	oxygen. Turb: to	urbidity. SpCon	d: specific cond	uctivity. Chl-a:	chlorophyll a. 1	$\tau$ : travel time fro	m upstream
	, ,	,									

concentration and observed DO concentration over the entire reach (i.e., mean of  $[DO]_{US,t-\frac{\tau}{2}}$  and  $[DO]_{DS,t+\frac{\tau}{2}}$ ).

Nighttime ecosystem respiration (ER) is equivalent to nighttime NEP, assuming no primary production occurs at night. Daytime ER was calculated from mean nighttime NEP, and thus GPP was calculated as the sum of NEP and ER during the daytime (Bott, 2007; Roberts et al., 2007). Assuming that net primary production (NPP) equals half of GPP (Odum, 1957) and net photosynthetic quotient as one (i.e., 1 mol O<sub>2</sub> release with 1 mol CO<sub>2</sub> consumption), areal autotrophic assimilation uptake  $(U_A)$  was estimated from NPP and the stoichiometric C:N molar ratios of biofilm, which have been measured in each reach (Junge et al., 2005; Kamjunke et al., 2015) (Equation 3). The stoichiometric C:N molar ratios used were 7 and 9 for May and September in Weiße Elster, respectively, and 9.4 for the Bode. After subtracting the inferred  $U_A$  from  $U_{NET}$ , we interpreted the remaining part as heterotrophic uptake  $U_D$ , which reflects the inverse heterotrophic uptake (dissimilation via denitrification and heterotrophic assimilation) and release (e.g., nitrification and remineralization) processes (Equation 4). Positive and negative  $U_D$  indicated the dominance of heterotrophic net NO<sub>3</sub>-N uptake and net NO<sub>3</sub>-N release, respectively.

$$U_{A,t} = \frac{GPP_t}{4.57 \times C : N} \tag{3}$$

$$U_{D,t} = U_{NET,t} - U_{A,t} \tag{4}$$

Because the original high-frequency measurements fluctuated greatly, we aggregated all data to hourly means for further analysis after all calculations. All calculations and statistical analyses (e.g., the ANOVA test) were performed using R software (Core Development Team, 2020).

## 3. Results

## 3.1. High-Frequency Measurements of Stream Water Hydrological and **Physiochemical Characteristics**

The high-frequency measurements of water-quality parameters showed large variations across reaches, as well as across campaigns within each reach (Table 2 and Table S4 in Supporting Information S1). For the two reaches in the Weiße Elster (WE\_1 and WE\_2), although all campaigns were conducted during the low-flow period, Q in May 2019 was nearly two times higher than in September 2019. This likely contributed to the higher turbidity observed in May than in September. Within each reach, NO3-N concentrations were similar in May and September, while between the two reaches, concentrations were slightly higher in the upstream reach WE\_1 than in the downstream reach WE\_2. Water temperature in May was ca. 2°C lower than that in September for each reach, and that of WE\_1 was generally lower than that of WE\_2. DO concentrations were similar during all four campaigns (mean of ca. 10 mg L<sup>-1</sup>), with slightly higher DO concentration and saturation percentage in May than in September for both reaches. Water pH and specific conductivity were significantly higher in WE\_2 than in WE\_1, and were significantly higher in September than in May for each reach. Chl-a was significantly higher in May than in September for WE\_1, but the opposite for WE\_2.

Water parameters had similar seasonal patterns during the five campaigns conducted over 3 years in the upper two reaches of the Bode River (BD\_1 and BD\_2). Discharge and associated turbidity decreased from June to August as the watershed continuously became dryer (Figure S1 in Supporting Information S1).

Table 3
Summary of Daily Mean Whole-Stream Metabolism and In-Stream N-Uptake Processes

		WE_1		WE_2		BD_1		BD_2			BD_3	
Processes	Units	2019–05	2019–09	2019–05	2019–09	2019–06	2020-08	2019–06	2020-08	2021–07	2019–08	2020–08
GPP	$g O_2 m^{-2} d^{-1}$	2.7	1.7	2.8	2.2	0.8	0.7	1.6	1.1	1.8	4.1	4.6
ER	${\rm g} \; {\rm O}_2 \; {\rm m}^{-2} \; {\rm d}^{-1}$	-1.6	-2.5	-1.2	-3.6	-3.3	-1.6	-3.7	-2.0	-2.5	-2.3	-3.2
$U_{\it NET}$	$mg\;N\;m^{-2}\;d^{-1}$	-151.1	-30.5	319.6	33.7	-100.8	-61.2	357.8	53.6	130.9	133.7	86.8
$U_{A}$	$mg \ N \ m^{-2} \ d^{-1}$	83.9	41.1	86.4	53.0	18.6	16.4	37.1	24.7	40.9	95.2	106.1
$U_D$	$mg \ N \ m^{-2} \ d^{-1}$	-235.0	-71.5	233.2	-19.3	-119.4	-77.6	320.7	28.8	90.0	38.5	-19.3

NO $_3$ <sup>-</sup>N concentrations decreased slightly from June (>1.60 mg L $^{-1}$ ) to August (<1.34 mg L $^{-1}$ ). Water temperature was similar during all campaigns (17.0–21.7°C). DO concentrations and saturation percentages were also similar, except for campaign 2020-08 BD $_2$ , which had significantly lower values (ANOVA test, p < 0.05). The pH was higher in June than in August. Conversely, *Chl-a* was significantly lower in June than in August (means of 2.15 and 2.85 µg L $^{-1}$ ; ANOVA test, p < 0.05), except for the much lower concentrations (<1.6 µg L $^{-1}$ ) during campaign 2021-07 BD $_2$ 2.

The behavior of the downstream reach of the Bode River (BD\_3) varied due to inputs from the upstream confluences of the Holtemme River and the lowland tributary Großer Graben (Figure 1), which are impacted greatly by urban wastewater and intensive lowland agriculture, respectively. Both campaigns were conducted in August, with similar environmental conditions for Q, NO<sub>3</sub><sup>-</sup>-N concentration, DO concentration and pH. However, water temperature and Chl-a concentration during the campaign in 2020 (16.18–17.03°C and 2.57  $\mu$ g L<sup>-1</sup>, respectively) were much lower than those in 2019 (17.49–20.04 and 4.46  $\mu$ g L<sup>-1</sup>, respectively).

## 3.2. Whole-Stream Metabolism and NO<sub>3</sub><sup>-</sup>-N Uptake Processes Across Reaches

Among all 11 campaigns, GPP showed consistent diel patterns, but with large variations across campaigns (Table 3; Figure 2). For the two reaches in the Weiße Elster (WE\_1 and WE\_2), GPP in May was significantly higher than that in September, whereas the absolute value of ER was significantly lower (ANOVA test, p < 0.05). For the middle Bode reach BD\_1, GPP was similar during the campaigns in June 2019 and August 2020 (ca. 0.7 g  $O_2$  m<sup>-2</sup> d<sup>-1</sup>), while the absolute ER of the former was twice as high as that of the latter (3.3 vs. 1.6 g  $O_2$  m<sup>-2</sup> d<sup>-1</sup>). In BD\_2, mean GPP was the lowest in August 2020 and was similar in June 2019 and July 2021 (1.1–1.8 g  $O_2$  m<sup>-2</sup> d<sup>-1</sup>). Mean ER was also the lowest in August 2020 and the highest in June 2019 (2.0–3.7 g  $O_2$  m<sup>-2</sup> d<sup>-1</sup>). For the most downstream reach (BD\_3), the GPP of the two August campaigns in 2019 and 2020 was similar and among the highest of all campaigns.

Patterns of  $NO_3^--N$  concentrations and net  $NO_3^--N$  uptake  $(U_{NET})$  in the 11 campaigns differed significantly across reaches, as well as among campaigns in the same reach (Table 3; Figure 3). In the Weiße Elster River, mean autotrophic assimilation uptake  $(U_A)$  in May was higher than that in September in both reaches. Reach WE\_2 showed continuously positive  $U_{NET}$  during both campaigns, but only the campaign in May 2019 showed positive  $U_D$ . In the Bode River, the two campaigns in BD\_1 showed negative  $U_{NET}$ . In BD\_2, the campaigns in June 2019 and July 2021 showed continuously positive  $U_{NET}$ , while in August 2020,  $U_{NET}$  was lowest and negative for several mid-day hours (with mean value of 53.6 mg N m<sup>-2</sup> d<sup>-1</sup>). In the most downstream reach (BD\_3), continuously positive  $U_{NET}$  was observed during the two August campaigns; however, only the campaign in 2019 had positive  $U_D$ .

## 3.3. NO<sub>3</sub><sup>-</sup>-N Uptake Pathways and Their Diel Variations

The mass-balance based  $U_{NET}$  were partitioned into  $U_A$  and  $U_D$  at the sub-daily scale (Figure 4). Except for campaigns in WE\_1 and BD\_1, most campaigns exhibited  $U_{NET} > 0$  (i.e., net NO<sub>3</sub>-N uptake), while their net uptake rates varied greatly (the daily mean  $U_{NET}$  ranged from 33.7 mg N m<sup>-2</sup> d<sup>-1</sup> during the 2019-09 WE\_2 campaign to 357.8 mg N m<sup>-2</sup> d<sup>-1</sup> during the 2019-06 BD\_2 campaign). In general, the net uptake was the highest in May-June post-wet season campaigns (Figures 4c and 4i), with generally much lower values in July-August

ZHANG ET AL. 7 of 17

1944/9793, 2023, 3, Downloaded from https://agupubs.onlinelibrary.wiley.com/doi/10.1029/2022WR032329, Wiley Online Library on [16/03/2023]. See the Terms and Conditions (https://onlinelibrary.wiley.com/terms-and-conditions) on Wiley Online Library for rules of use; OA articles are governed by the applicable Creative Commons Licenses

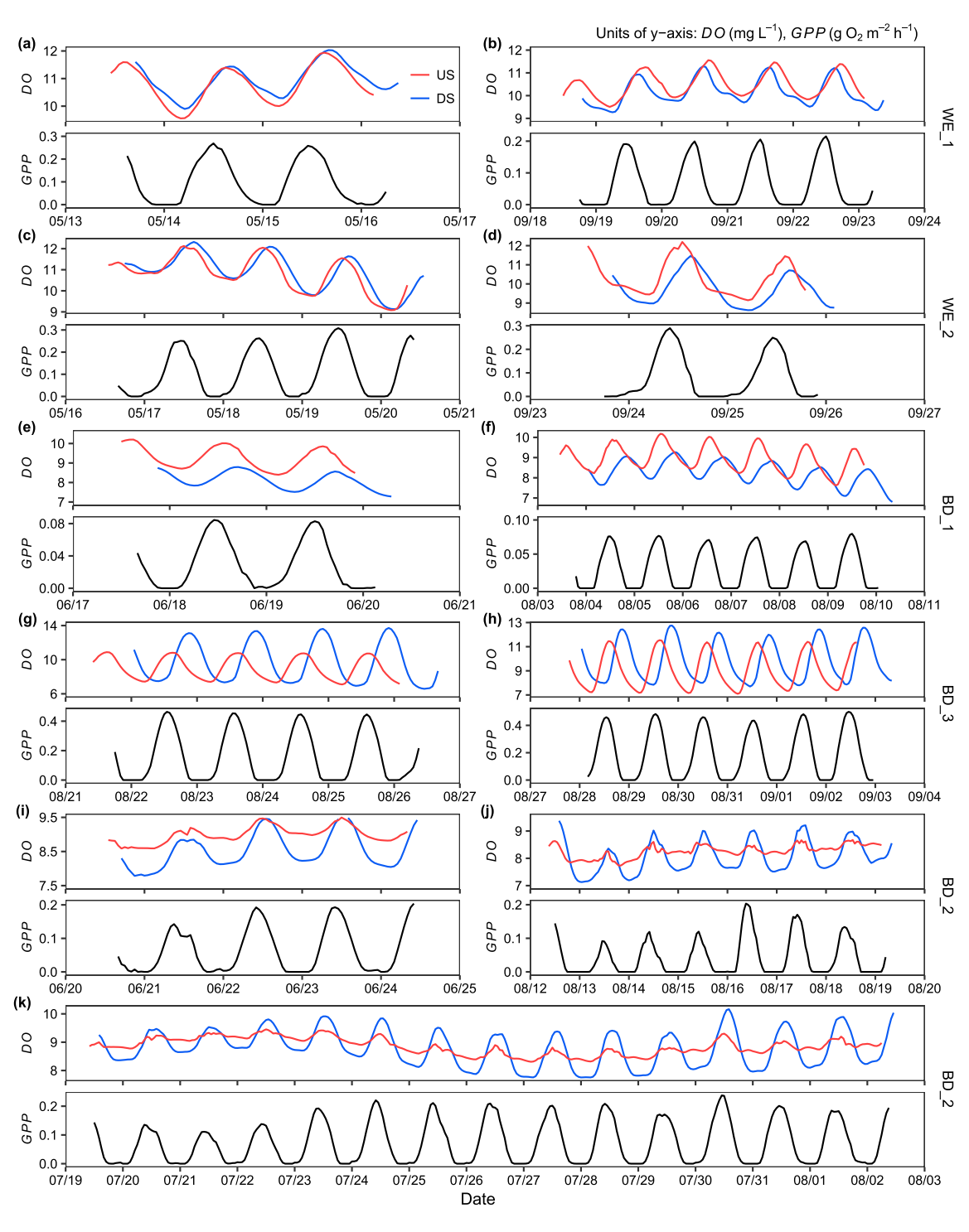


**Figure 2.** Time series of dissolved oxygen concentrations (mg  $L^{-1}$ , the upper panel of each subplot) at the upstream (US) and downstream (DS) stations, and the two-station based gross primary production (GPP, g  $O_2$  m<sup>-2</sup> h<sup>1</sup>, the lower panel of each subplot) for each of all campaigns at reaches WE\_1 (a) and (b), WE\_2 (c) and (d), BD\_1 (e) and (f), BD\_3 (g) and (h) and BD\_2 (i)–(k).

campaigns (Figures 4g, 4j and 4k) and the lowest in late August and September dry season campaigns (Figures 4d and 4h). Moreover,  $U_{NET}$  was dominated mainly by  $U_D$  rather than  $U_A$  during the post-wet seasons, with  $U_D$  accounting for 90% and 73% of  $U_{NET}$  throughout the 2019-06 BD\_2 and 2019-05 WE\_2 campaigns, respectively. Interestingly, for the three campaigns in BD\_2,  $U_{NET}$  decreased substantially from June to August, associated with decreasing  $U_D$  uptake (mostly >0) proportions and increasing  $U_A$  proportions (Figures 4i-4k). The

ZHANG ET AL. 8 of 17

1944/9793, 2023, 3, Downloaded from thtps://agupubs.onlinelibrary.viely.com/doi/10.1029/2022WR032329, Wiley Online Library on [16/03/2023], See the Terms and Conditions (https://onlinelibrary.wiley.com/terms-and-conditions) on Wiley Online Library for rules of use; OA articles are governed by the applicable Creative Conditions (https://onlinelibrary.wiley.com/terms-and-conditions) on Wiley Online Library for rules of use; OA articles are governed by the applicable Creative Conditions (https://onlinelibrary.wiley.com/terms-and-conditions) on Wiley Online Library for rules of use; OA articles are governed by the applicable Creative Conditions (https://onlinelibrary.wiley.com/terms-and-conditions) on Wiley Online Library for rules of use; OA articles are governed by the applicable Creative Conditions (https://onlinelibrary.wiley.com/terms-and-conditions) on Wiley Online Library for rules of use; OA articles are governed by the applicable Creative Conditions (https://onlinelibrary.wiley.com/terms-and-conditions) on Wiley Online Library for rules of use; OA articles are governed by the applicable Creative Conditions (https://onlinelibrary.wiley.com/terms-and-conditions) on Wiley Online Library for rules of use; OA articles are governed by the applicable Creative Conditions (https://onlinelibrary.wiley.com/terms-and-conditions) on Wiley Online Library for rules of use; OA articles are governed by the applicable Creative Conditions (https://onlinelibrary.wiley.com/terms-and-conditions) on Wiley Online Library for rules of use; OA articles are governed by the applicable Creative Conditions (https://onlinelibrary.wiley.com/terms-and-conditions) on Wiley Online Library for rules of use; OA articles are governed by the applicable Creative Conditions (https://onlinelibrary.wiley.com/terms-and-conditions) on Wiley Online Library for rules of use; OA articles are governed by the applicable Creative Conditions (https://onlinelibrary.wiley.com/terms-and-conditions) on the applicable Creative Conditions (https://onlinelibrary.w

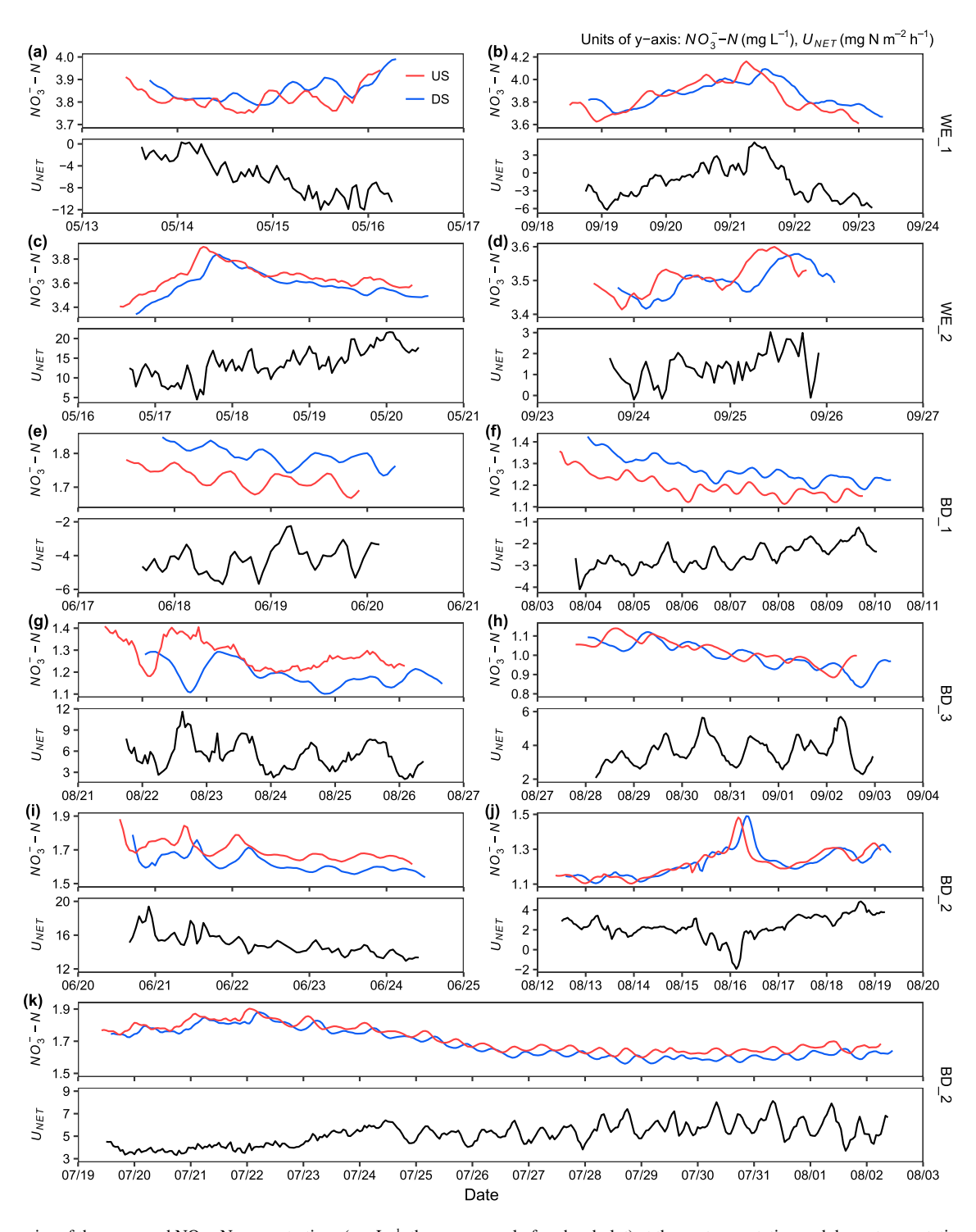


Figure 3. Time series of the measured  $NO_3^-N$  concentrations (mg  $L^{-1}$ , the upper panel of each subplot) at the upstream station and downstream stations and the two-station based areal net  $NO_3^-N$  uptake ( $U_{NET}$ , mg N m<sup>-2</sup> h<sup>-1</sup>, the lower panel of each subplot) for each of all campaigns at reaches WE\_1 (a) and (b), WE\_2 (c) and (d), BD\_1 (e) and (f), BD\_3 (g) and (h) and BD\_2 (i)–(k).

absolute uptake rates of  $U_A$  were similar, while  $U_{NET}$  was significantly lower in July and August (i.e., 53.6 and 130.9 mg N m<sup>-2</sup> d<sup>-1</sup>, respectively), resulting in dramatical decreases of  $U_D$  uptake rates, with even few negative values occurred during the mid-day hours in August (indicating net N release). Such decreased  $U_D$  and its further diurnal shift between uptake and release ( $U_D$  cross zero) were ubiquitously observed in our campaigns that have been conducted in dry seasons (see most of August and September campaigns in Figure 4).

ZHANG ET AL. 9 of 17

1944 9793, 2023, 3, Downloaded from https://agupubs.onlinelibrary.wiley.com/doi/10.1029/2022WR033329, Wiley Online Library on [16/03/2023]. See the Terms and Conditions (https://onlinelibrary.wiley.com/terms-and-conditions) on Wiley Online Library for rules of use; OA articles are governed by the applicable Creative Coreaive Coreaive

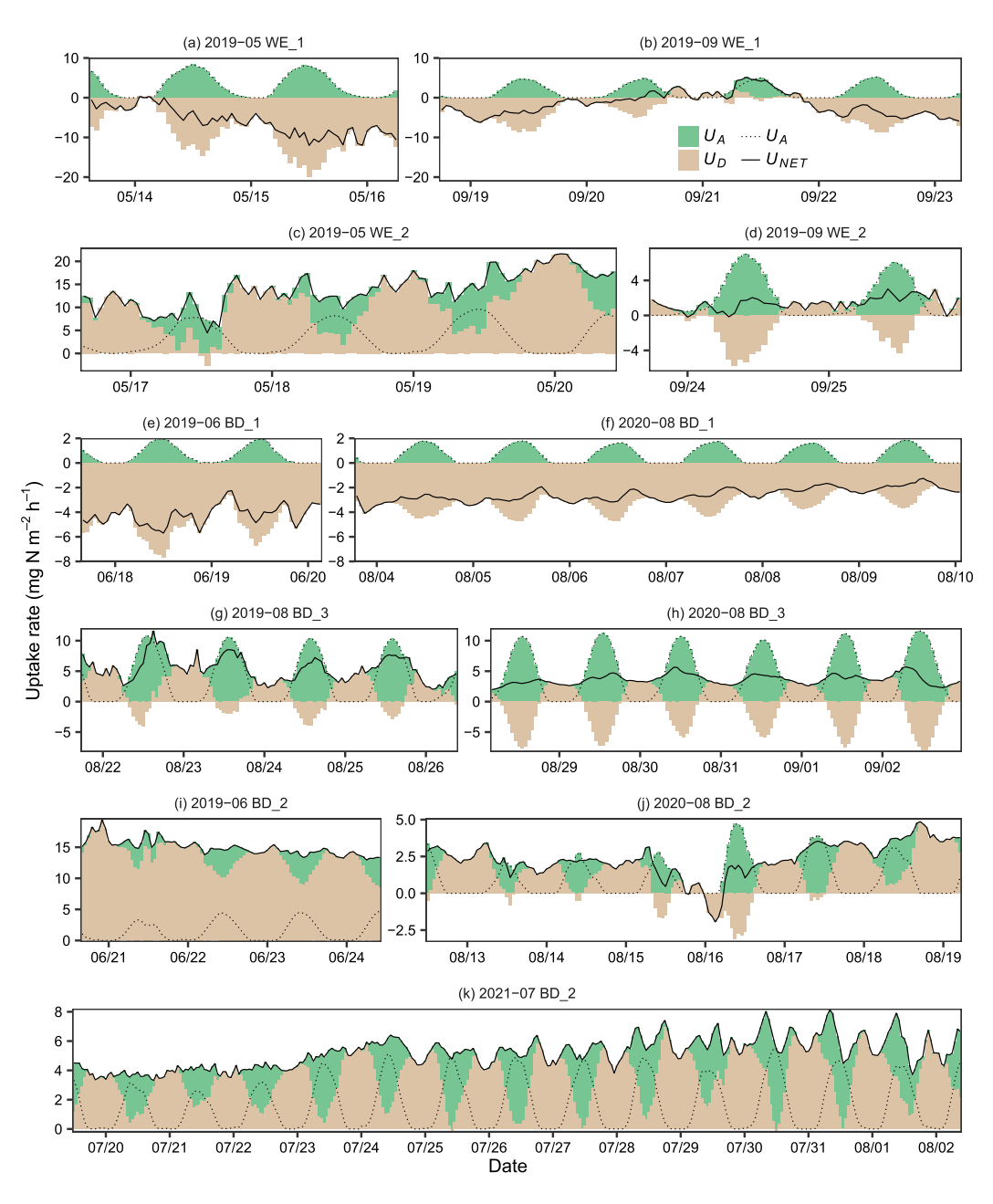


Figure 4. Sub-daily time series of the disentangled  $NO_3^-$ -N uptake pathways in all 11 campaigns. The overall net  $NO_3^-$ -N uptake  $(U_{NET})$  rates were partitioned into autotrophic assimilation uptake  $(U_A)$ , green colored area) and heterotrophic uptake  $(U_D)$ , brown colored area). Note that negative  $U_{NET}$  indicates net  $NO_3^-$ -N release within the monitored reach, and negative  $U_D$  represents.

The four campaigns conducted in WE\_1 and BD\_1 reaches (Figures 4a-b and 4e-f, respectively) showed ubiquitous negative  $U_{NET}$  (i.e., net NO<sub>3</sub><sup>-</sup>-N release), and the releasing rate of campaigns during post-wet seasons was generally higher than that of campaigns during dry seasons for the same reach.

In addition to the seasonal and cross-reach variations,  $U_{NET}$  also showed various diel patterns across campaigns. For instance, during the daytime,  $U_{NET}$  decreased to its diurnal minima in campaigns 2019-05 WE\_2 and 2021-07 BD\_2 (Figures 4c and 4k) while increasing to diurnal maxima during the 2019-08 BD\_3 campaign (Figure 4g). For campaigns with  $U_{NET} < 0$ , the net  $NO_3^-$ -N release also varied diurnally, likely increasing during the daytime (e.g., Figures 4a and 4e).

ZHANG ET AL. 10 of 17

9447973, 2023, 3, Downloaded from https://agupubs.onlinelibrary.wiley.com/doi/10.1029/2022WR032329, Wiley Online Library on [16/03/2023]. See the Terms

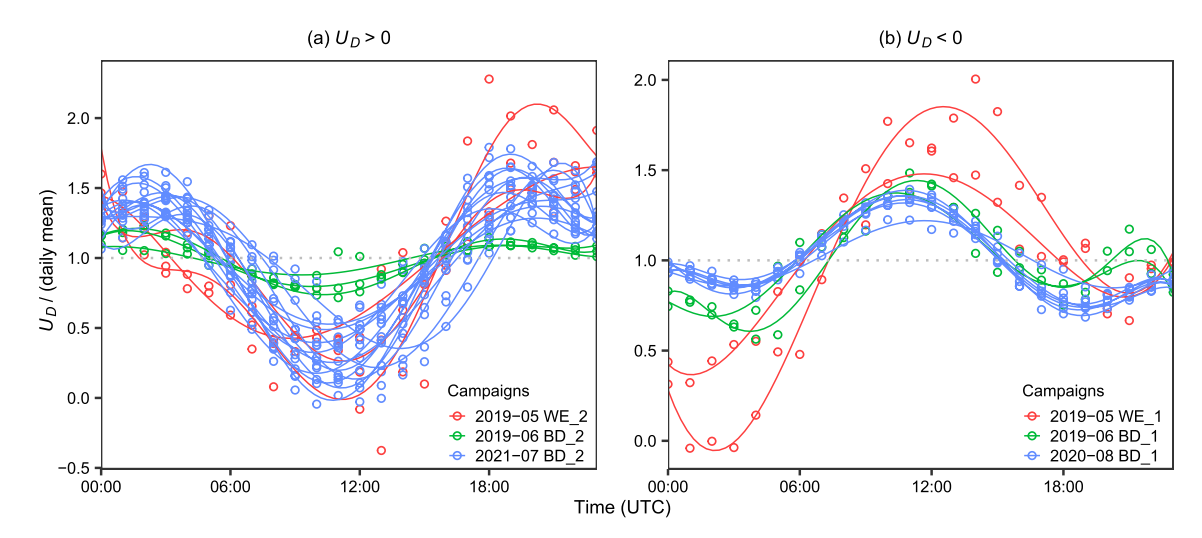


Figure 5. Diel patterns of the subtracted  $U_D$ . The rescaled  $U_D$  in y-axes were calculated as hourly  $U_D$  divided by the mean values in each day. Note that here we only showed campaigns exhibiting consistent heterotrophic uptake  $U_D > 0$  (a) or release  $U_D < 0$  (b).

As the remaining part of subtracting  $U_A$  from  $U_{NET}$ ,  $U_D$  exhibited distinct diel signals (Figure 5). For campaigns with consistent  $U_D > 0$  in Figure 5a, the heterotrophic  $NO_3^-N$  uptake exhibited an obvious decreasing diel pattern (i.e., the minima occurred during the daytime) because  $U_{NET}$  did not increase equally with the increases of  $U_A$  and sometimes even decreased significantly. In contrast, for campaigns with consistent  $U_D < 0$  in Figure 5b, the nitrification N release increased during the daytime, accompanied by the higher day-time net release (i.e., higher values of  $|U_{NET}|$  shown in Figure 4). Interestingly, despite the large variability of  $U_D$ , the relative degrees of its diel variations (i.e., hourly  $U_D$  rescaled by the mean of each day) were largely consistent within a campaign duration (Figure 5), and similar across reaches (e.g., campaigns 2019-08 WE\_2 and 2021-07 BD\_2) and seasons (e.g., the June and August campaigns in BD\_1). Also, it is worth noting that such diel variations could be largely masked when net uptake rates were very high (e.g., up to ca. 357 mg N m<sup>-2</sup> d<sup>-1</sup> in campaign 2019-06 BD\_2, right after a moderate flow event, Figure S2 in Supporting Information S1) or be affected by dramatic changes of stream environments (e.g., water temperature decreased by 2°C and specific conductivity increased by 100  $\mu$ S cm<sup>-1</sup> during the second day of campaign 2019-05 WE\_1, Figure S5a in Supporting Information S1).

## 4. Discussion

# 4.1. Stream Metabolism and the Informed Autotrophic N Assimilation $\,$

During the 11 campaigns, DO concentrations showed clear diel patterns that generally peaked near midday. At the downstream station of reaches BD\_1 and BD\_3, DO peaked near midnight, with a consistent time lag compared to the upstream DO peaks (Figure 2). Artificial channel weirs were located ca. 700 m downstream of both downstream stations, which might have induced impoundment effects that slowed the flow velocity and decreased the reaeration rate (Churchill et al., 1964) (see also Table 2). GPP can be higher in the afternoon than in the morning with similar radiation due to higher temperatures at the cellular level (Beaulieu et al., 2013) or changes in the influence of riparian vegetation shading due to channel orientation (azimuth) (Julian et al., 2008). Moreover, in high-order reaches, complex hydraulic characteristics (e.g., dispersion and transient storage) and their impacts on transport and distortion of DO signals can affect direct inferences of stream metabolism even when using the two-station method (Hensley & Cohen, 2016). Future research could be oriented to further integrate high-frequency data analysis with hydraulic simulations.

Estimates of GPP varied greatly among the 11 campaigns (ranged between 0.7 and 4.6 g  $O_2$  m<sup>-2</sup> d<sup>-1</sup>, Table 3), primarily due to combined effects of multiple environmental controls (e.g., varying radiation across seasons and varying riparian shading across different reaches). Based on the stoichiometric conversion (Equation 3), this directly generated the high variability of inferred  $NO_3^-$ -N uptake by autotrophic assimilation ( $U_A$ ) among our campaigns (ranged between 16.4 and 106.1 mg N m<sup>-2</sup> d<sup>-1</sup>). Although widely applied in literature, such stoichiometric relationships need to be cautiously verified for specific sites, especially at sub-daily time scales.

ZHANG ET AL. 11 of 17

We obtained C:N molar ratios from local biofilm measurements (Junge et al., 2005; Kamjunke et al., 2015). The derived 42.9 g  $O_2$  per g N assimilation in the Bode River (4.57 × 9.4 in Equation 3) was comparable with regression slopes of 38.8 and 36.6 at the Hausneindorf site (8 km south of the BD\_1) where  $U_A$  was directly inferred from diel amplitudes of  $NO_3$ -N concentrations during low-flows (see Rode, Halbedel Née Angelstein et al. (2016) and Yang et al. (2019)).

## 4.2. Nitrate Transport and Uptake Processes

Unlike the consistent diel patterns of DO,  $NO_3^--N$  concentrations varied greatly among campaigns. The expected diel pattern of  $NO_3^--N$  concentrations decreases to minima during the daytime due to assimilation uptake  $U_A$  (Heffernan & Cohen, 2010; Rode, Halbedel Née Angelstein et al., 2016) was rarely observed at individual stations. Compared to upstream perturbations of gaseous-based DO (e.g., variable tributaries and effluents), those of non-gaseous  $NO_3^-$  signals persist much longer due to the lack of atmospheric equilibration, which obscures the diel uptake signals using one-station inferences (Hensley & Cohen, 2016). This agrees with previous one-station-based studies that observed clear diel signals mostly under steady upstream input (e.g., in springfed rivers (Heffernan & Cohen, 2010)) or during low-flow summer periods (Rode, Halbedel Née Angelstein et al., 2016). Such methodological limitations can be largely relaxed using the two-station method, such as the present study, to extract diel patterns of in-stream  $NO_3^-$ -N uptake from the change between upstream and down-stream  $NO_3^-$ -N signals.

Our estimates of NO<sub>2</sub>-N uptake based on two-station measurements showed high spatiotemporal variability. One reason could be differing degrees of hydro-biochemical connectivity between river channels and off-channel storage zones. Flow pathways from different sub-ecosystem compartments converge along the river network. The varying residence times, contacting volumes, and stream substrates also create spatial and temporal variations in biogeochemical reactions (Anlanger et al., 2021; Harvey et al., 2019). Net  $NO_3$ -N uptake ( $U_{NET}$ ) during the 2019-05 WE\_2 campaign was among the highest, potential because this was a more natural stream reach and occurred right after the annual wet season (Figure 1; Table 1). It is widely reported that more natural stream reaches can retain more nutrients than highly modified reaches (Hall et al., 2009; Hester et al., 2018; Sweeney et al., 2004). Moreover, other compartments (e.g., adjacent riparian corridors, floodplains, the hyporheic zone) could be more active along natural reaches, which could be important N sinks involving high rates of assimilation (by both autotrophs and heterotrophs) and dissimilation (e.g., denitrification) uptake (Helton et al., 2011; Mulholland et al., 2008). Notably, the heterotrophic uptake  $(U_D)$  pathway represented ca. 73% of  $U_{NET}$  during this campaign, indicating that heterotrophic uptake processes (including assimilation by heterotrophs and dissimilation via denitrification) were active during the post-wet seasons (May-June). This phenomenon was clear when comparing June 2019 and July 2021 campaigns to reach BD 2 ( $U_D$  accounted for 90% and 69% of total uptake, respectively, Figures 4i and 4k), in which the former was conducted immediately after a high-flow event receded (Figure S2b in Supporting Information S1). High discharge during the wet season can deliver large amounts of fresh organic matter to river networks, especially the labile fraction, which can greatly increase biogeochemical activity (Fellman et al., 2009; Tesi et al., 2008), and denitrification can be promoted by vertical turbulent mixing of hyporheic sediments (Harvey et al., 2019). Moreover, mean Chl-a concentration increased greatly from 15 April (5.67  $\mu g L^{-1}$ ) to the beginning of July 2019 (9.85  $\mu g L^{-1}$ ) (see Figure S10 in Supporting Information S1 for long-term in-situ monitoring data at station GGL (52°00'03" N, 11°21'21" E) close to the upstream site of BD\_3). Increasing stream water temperature was unlikely to be responsible for such uptake variations since it was already >10°C in late spring and early summer (data from station GGL), and the temperature during all campaigns (Table 2) was likely sufficient to ensure active biogeochemical reactions (Dawson & Murphy, 1972).

Estimating complex lateral subsurface seepage into rivers is challenging, especially in flat-topographic lowland regions with heavily human-altered landscapes. Despite the considerations taken in our study design, unaccounted lateral inflows may influence our uptake estimates. In the case of BD\_1 reach, for instance, estimates of  $U_{NET}$  were consistently negative (Figures 4e and 4f). We note that (a) the DEM-derived drainage network diverts largely from the artificially modified channels in the lower part of the sub-catchment (Figure S3 in Supporting Information S1) and (b) the steep gradients of the groundwater table suggest complex groundwater dynamics (data from LHW groundwater wells, Figure S4 in Supporting Information S1). Nevertheless, there remain several ways of detecting the potential impacts of such lateral inputs. Changes in specific conductivity along the reach can indicate additional water sources other than upstream inputs. For instance, the consistently higher values at

ZHANG ET AL. 12 of 17



the downstream station than the upstream station of BD\_1 (Figure S7 in Supporting Information S1) directly supported the inference of substantial unaccounted-for lateral inflows from groundwater seepage along the BD\_1 reach. The two WE reaches, in contrast, showed marginal differences in specific conductivity between upstream and downstream stations, confirming that lateral inflows had negligible influence on mass balance calculations.

Given the well-recognized retentive capacity of streams, the negative values of  $U_{NET}$  in particular, need to be critically interpreted. On the one hand, the higher downstream N loads might result from underestimated lateral inputs. This would be particularly the case for reaches exhibiting consistent negative values (e.g., the above discussed BD\_1 reach). On the other hand, the negative values could be caused by actual  $NO_3^-$  release from stream organic storage with short turnover times (e.g., re-mineralization and nitrification). These transformations depend greatly on  $NH_4^+$  concentration, substrate types, and organic carbon (Bernhardt et al., 2002; Day & Hall, 2017; Kemp & Dodds, 2002). Any production of  $NO_3^-$  by nitrification would offset decreases in  $NO_3^-$  concentrations from uptake, resulting in a decrease in  $U_{NET}$  or even a negative value in cases where the former is larger than the latter (Jarvie et al., 2018).

## 4.3. Heterogeneous Diel Variations in Nitrate Uptake Pathways

We estimated autotrophic uptake ( $U_A$ ) from the GPP signal assuming a constant stoichiometric C:N ratio. Because of this, both the timing and magnitude of  $U_A$  is directly coupled with GPP. GPP always had a strong diel pattern (i.e., diel maxima during the daytime) during all campaigns (Figure 4) over a variety of radiation and riparian-shading conditions. While the temporal and stoichiometric coupling of autotrophic uptake with primary production is often assumed, it has been called into question by Appling and Heffernan (2014) and confirmed by Chamberlin et al. (2019). They suggest that de-coupling can occur at low nutrient concentrations, however, this is not the case in any of our study reaches. Moreover, we tested scenarios of  $U_A$  lagging 1–3 hr after GPP and observed that diel minima/maxima of the net uptake ( $U_{NET}$ ) were indeed delaying GPP maxima for some campaigns (e.g., 2019-08 BD\_3 and 2021-07 BD\_2, see details in Movie S1). We note that (a) the exact lag times were difficult to determine (not consistent across the 11 campaigns) and (b) the disentangled NO<sub>3</sub><sup>-</sup>-N uptake pathways and their temporal variability were not substantially altered in our time-lag scenario analysis. Of course, we note that this physiological time lag should be further evaluated, especially for studies focusing on the timing of diel signals.

The reasons for the inferred diel pattern in  $U_D$  are likely complex, involving the counterbalance of the inverse processes of heterotrophic  $NO_3^-$ -N uptake and  $NO_3^-$ -N release. For campaigns with consistent  $U_{NET} > 0$ , the decreasing diel signals (i.e., diel minima during the daytime) of  $U_D$  could have largely resulted from simply subtracting  $U_A$ . However, the directly measured  $U_{NET}$  often exhibited obvious and extensive decreasing during the daytime (e.g., the majority of dates during campaigns 2019-05 WE\_2 and 2021-07 BD\_2, Figures 4c and 4k, respectively). As  $U_A$  is normally expected to increase during the day, this provided direct evidence that the heterotrophic NO<sub>3</sub><sup>-</sup>-N uptake processes (for cases of  $U_D > 0$ , Figure 5a) were very likely decreasing during the daytime and contributing to diel variation in  $NO_3$ -N concentration. These diel patterns in  $U_D$  are often overlooked in reach-scale nutrient-removal studies, where diel variations in nutrient concentrations are assumed to result from  $U_A$  (Heffernan & Cohen, 2010) or from diurnal variation in lateral inflows (Hensley et al., 2015). Denitrification can become the dominant process in total NO<sub>2</sub><sup>-</sup>-N uptake as evidenced by measuring isotopes (Cohen et al., 2012). Experimental evidence has revealed that the denitrification rate can decrease at sunrise in the water column and sediment using an open-channel N<sub>2</sub> method (Reisinger et al., 2016); denitrification rates show large diel variations related to temperature in the hyporheic zone, as simulated by a physical model (Zheng & Bayani Cardenas, 2018). In addition, the decreasing  $U_D$  diel pattern (Figure 5a) could be influenced by the increase of DO during the daytime, since DO usually inhibits denitrification but stimulates nitrification, both having the same net effect on the decrease in NO<sub>3</sub>-N removal. Besides the influence of DO, the diel pattern could also have resulted from N fixation that can balance heterotrophic assimilation (Welsh et al., 2000), resulting in an overall decreasing pattern during the daytime. Although uncertainty may embed in cases with  $U_{NET} < 0$  (and consequently  $U_D < 0$ , Figure 5b), the diel pattern with maxima occurring during the daytime agreed well with the inferred N releasing processes (e.g., nitrification), which may be promoted by increasing DO and water temperature during the daytime (Gammons et al., 2011).

## 4.4. Further Perspectives of In-Stream Process Monitoring and Network Modeling

Benefiting from the flexibility of high-frequency, sensor-based monitoring, this study extended the two-station method of inferring in-stream NO<sub>3</sub><sup>-</sup>-N processes to higher-order reaches under varying environmental conditions.

ZHANG ET AL. 13 of 17

Combining direct measurements of stream metabolism and  $NO_3^-$ -N mass balance allowed for disentangling various  $NO_3^-$ -N uptake pathways and further investigating their spatiotemporal variability. In addition to the well-explored autotrophic assimilation  $U_A$  and the more intuitive component of  $U_{NET}$ , one of the major novelties of this study was to quantitatively infer the reach-scale  $U_D$ , which represents the net balance of inverse heterotrophic  $NO_3^-$ -N uptake (i.e., denitrification and heterotrophic assimilation) and  $NO_3^-$ -N release (i.e., nitrification/mineralization). Direct reach-scale measuring of  $U_D$  remains challenging, given its high spatiotemporal variability and diel variations at a sub-daily scale as indicated in this study. Further quantifying these multiple overlapping processes would require combining different kinds of measurements and model-based estimates. For example, isotopes can be added to further disentangle denitrification and provide information on spatial stream heterogeneity (Böhlke et al., 2004; Mulholland et al., 2008). Further information on in-stream biogeochemical processes, that is not measured but informative, can be derived from model-based estimates (e.g., Jarvie et al., 2018 obtained continuous estimates of dissolved inorganic carbon and  $CO_2$  release from the THINCARB model to support the inferred change in rates of microbial respiration).

This complexity of in-stream  $NO_3^--N$  processing has created challenges for network-scale modeling, as well as for catchment modeling that further involves terrestrial processes. Reach-scale monitoring and analysis, like this study, are able to provide pathway-specific quantifications (e.g., heterotrophic uptake  $U_D$  can reach up to 230–320 mg N m<sup>-2</sup> d<sup>-1</sup>, Table 3), which are still rare at larger scales. Such quantitative information can, at least, serve as invaluable reference values for verifying model estimates, which often employ highly simplified conceptualization and rely on model parameterization. By cross-comparing such information obtained under various conditions (different seasons and streams), insights into environmental controls on in-stream processes can be used to further derive new approaches of process regionalization, refining current models based largely on assumptions of first-order kinetics. For example, the parsimonious approach of quantifying autotrophic  $NO_3^-$ -N uptake by Yang et al. (2019) was derived from the contrasting seasonal patterns of GPP-related  $NO_3^-$ -N uptake in open- and closed-canopy reaches, and further upscaled to the river-network scale.

#### 5. Conclusion

High-frequency multi-parameter sensors have great potential to quantify reach-scale in-stream net  $NO_3^-$  uptake and to conduct detailed investigations of in-stream metabolism and coupled  $NO_3^-$  cycling pathways. The high-frequency data allowed us to calculate different uptake pathways at hourly time steps and to explore diel variations in these  $NO_3^-$ -N uptake pathways. The mass-balance based rates of net  $NO_3^-$ -N uptake varied seasonally and across stream conditions, and were highest in the more natural reach and during the post-wet seasons (May-June). Compared to assimilatory uptake ( $U_A$ ), heterotrophic uptake ( $U_D$ ) likely dominated net  $NO_3^-$ -N uptake during the post-wet seasons, but its proportion largely decreased during the dry season (August-September), often becoming negative (indicating net  $NO_3^-$ -N release). The inferred  $U_D$  also exhibited substantial diel patterns; if  $U_A$  is strictly coupled with GPP as is commonly assumed and yet no diurnal  $U_{NET}$  the signal is present, it suggests that  $U_D$  must decrease during the daytime, which has long been overlooked in previous studies. Overall, our approach and findings can provide new insights into heterogeneous dynamics of in-stream  $NO_3^-$  retention processes at larger scales.

## **Data Availability Statement**

The high-frequency monitoring data used are available at Zhang et al. (2022) via https://doi.org/10.48758/ufz.12911. The CORINE (2018) data used for identifying landscape type are available at the Federal Agency for Cartography and Geodesy (BKG) (https://gdz.bkg.bund.de/index.php/default/corine-land-cover-5-ha-stand-2018-clc5-2018.html). The discharge, groundwater, and river morphology data are available at the data portal (Datenportal) of the State Agency for Flood Protection and Water Management of Saxony Anhalt, Germany (LHW, 2022) (https://gld.lhw-sachsen-anhalt.de/).

ZHANG ET AL. 14 of 17

19447973, 2023, 3, Downloaded from https://agupubs

of use; OA articles

#### Acknowledgments

Xiaolin Zhang is funded by the Chinese Scholarship Council (CSC). We thank Uwe Kiwel for his technical support during the field work. We also thank the Federal Agency for Cartography and Geodesy (BKG) and the State Agency for Flood Protection and Water Management of Saxony Anhalt, Germany (LHW) for all data support. Open Access funding enabled and organized by Projekt DEAL.

## References

- Alberts, J. M., Beaulieu, J. J., & Buffam, I. (2017). Watershed land use and seasonal variation constrain the influence of riparian canopy cover on stream ecosystem metabolism. *Ecosystems*, 20(3), 553–567. https://doi.org/10.1007/s10021-016-0040-9
- Alexander, R. B., Smith, R. A., & Schwarz, G. E. (2000). Effect of stream channel size on the delivery of nitrogen to the Gulf of Mexico. *Nature*, 403(6771), 758–761. https://doi.org/10.1038/35001562
- Anlanger, C., Risse-Buhl, U., Schiller, D., Noss, C., Weitere, M., & Lorke, A. (2021). Hydraulic and biological controls of biofilm nitrogen uptake in gravel-bed streams. *Limnology & Oceanography*, 66(11), 3887–3900. https://doi.org/10.1002/lno.11927
- Appling, A. P., & Heffernan, J. B. (2014). Nutrient limitation and physiology mediate the fine-scale (de)coupling of biogeochemical cycles. *The American Naturalist*, 184(3), 384–406. https://doi.org/10.1086/677282
- Arango, C. P., Tank, J. L., Johnson, L. T., & Hamilton, S. K. (2008). Assimilatory uptake rather than nitrification and denitrification determines nitrogen removal patterns in streams of varying land use. *Limnology & Oceanography*, 53(6), 2558–2572. https://doi.org/10.4319/lo.2008.53.6.2558
- Beaulieu, J. J., Arango, C. P., Balz, D. A., & Shuster, W. D. (2013). Continuous monitoring reveals multiple controls on ecosystem metabolism in a suburban stream. Freshwater Biology, 58(5), 918–937. https://doi.org/10.1111/fwb.12097
- Bernhardt, E. S., Hall, R. O., & Likens, G. E. (2002). Whole-system estimates of nitrification and nitrate uptake in streams of the Hubbard Brook Experimental Forest. *Ecosystems*, 5(5), 419–430. https://doi.org/10.1007/s10021-002-0179-4
- Billen, G., Garnier, J., & Lassaletta, L. (2013). The nitrogen cascade from agricultural soils to the sea: Modelling nitrogen transfers at regional watershed and global scales. *Philosophical Transactions of the Royal Society B: Biological Sciences*, 368(1621), 20130123. https://doi.org/10.1098/rstb.2013.0123
- Böhlke, J. K., Harvey, J. W., & Voytek, M. A. (2004). Reach-scale isotope tracer experiment to quantify denitrification and related processes in a nitrate-rich stream, midcontinent United States. Limnology & Oceanography, 49(3), 821–838. https://doi.org/10.4319/LO.2004.49.3.0821
- Bott, T. L. (2007). Primary productivity and community respiration. In *Methods in stream ecology* (2nd ed., pp. 663–690). Elsevier. https://doi.org/10.1016/B978-012332908-0.50040-1
- Burns, D. A., Pellerin, B. A., Miller, M. P., Capel, P. D., Tesoriero, A. J., & Duncan, J. M. (2019). Monitoring the riverine pulse: Applying high-frequency nitrate data to advance integrative understanding of biogeochemical and hydrological processes. Wiley Interdisciplinary Reviews: Water, 6(4), e1348. https://doi.org/10.1002/wat2.1348
- Chamberlin, C. A., Bernhardt, E. S., Rosi, E. J., & Heffernan, J. B. (2019). Stoichiometry and daily rhythms: Experimental evidence shows nutrient limitation decouples N uptake from photosynthesis. *Ecology*, 100(10), e02822. https://doi.org/10.1002/ecy.2822
- Chamberlin, C. A., Katul, G. G., & Heffernan, J. B. (2021). A multiscale approach to timescale analysis: Isolating diel signals from solute concentration time series. *Environmental Science & Technology*, 55(18), 12731–12738. https://doi.org/10.1021/acs.est.1c00498
- Chapra, S. C., & Di Toro, D. M. (1991). Delta method for estimating primary production, respiration, and reaeration in streams. *Journal of Environmental Engineering*, 117(5), 640–655. https://doi.org/10.1061/(asce)0733-9372(1991117:5(640)
- Churchill, M. A., Elmore, H. L., & Buckingham, R. A. (1964). The Prediction of stream reaeration rates. Advances in Water Pollution Research, 89–136. https://doi.org/10.1016/b978-1-4832-8391-3.50015-4
- Cohen, M. J., Heffernan, J. B., Albertin, A., & Martin, J. B. (2012). Inference of riverine nitrogen processing from longitudinal and diel variation in dual nitrate isotopes. *Journal of Geophysical Research*, 117(1), 1021. https://doi.org/10.1029/2011JG001715
- Core Development Team, R. (2020). A Language and environment for statistical Computing. R Foundation for Statistical Computing. Retrieved from http://www.r-project.org
- CORINE. (2018). CORINE land Cover 5 ha, Stand 2018 (CLC5-2018). [Dataset]. Federal Agency for Cartography and Geodesy (BKG). accessed 1/19/2023. Retrieved from https://gdz.bkg.bund.de/index.php/default/open-data/corine-land-cover-5-ha-stand-2018-clc5-2018.html
- Covino, T. P., McGlynn, B. L., & McNamara, R. A. (2010). Tracer additions for spiraling curve characterization (TASCC): Quantifying stream nutrient uptake kinetics from ambient to saturation. *Limnology and Oceanography: Methods*, 8(SEPT), 484–498. https://doi.org/10.4319/lom.2010.8.484
- Dawson, R. N., & Murphy, K. L. (1972). The temperature dependency of biological denitrification. Water Research, 6(1), 71–83. https://doi.org/10.1016/0043-1354(72)90174-1
- Day, N. K., & Hall, R. O. (2017). Ammonium uptake kinetics and nitrification in mountain streams. Freshwater Science, 36(1), 41–54. https://doi.org/10.1086/690600
- Demars, B. O. L., Russell Manson, J., Ólafsson, J. S., Gíslason, G. M., Gudmundsdóttir, R., Woodward, G., et al. (2011). Temperature and the metabolic balance of streams. Freshwater Biology, 56(6), 1106–1121. https://doi.org/10.1111/j.1365-2427.2010.02554.x
- Fellman, J. B., Hood, E., D'Amore, D. V., Edwards, R. T., & White, D. (2009). Seasonal changes in the chemical quality and biodegradability of dissolved organic matter exported from soils to streams in coastal temperate rainforest watersheds. *Biogeochemistry*, 95(2), 277–293. https:// doi.org/10.1007/s10533-009-9336-6
- Fowler, D., Coyle, M., Skiba, U., Sutton, M. A., Cape, J. N., Reis, S., et al. (2013). The global nitrogen cycle in the twenty-first century. *Philosophical Transactions of the Royal Society B: Biological Sciences*, 368(1621), 20130164. https://doi.org/10.1098/rstb.2013.0164
- Friese, K., Schultze, M., Boehrer, B., Büttner, O., Herzsprung, P., Koschorreck, M., et al. (2014). Ecological response of two hydro-morphological similar pre-dams to contrasting land-use in the Rappbode reservoir system (Germany). *International Review of Hydrobiology*, 99(5), 335–349. https://doi.org/10.1002/iroh.201301672
- Gammons, C. H., Babcock, J. N., Parker, S. R., & Poulson, S. R. (2011). Diel cycling and stable isotopes of dissolved oxygen, dissolved inorganic carbon, and nitrogenous species in a stream receiving treated municipal sewage. *Chemical Geology*, 283(1), 44–55. https://doi.org/10.1016/j.chemseo.2010.07.006
- Gomez-Velez, J. D., Harvey, J. W., Cardenas, M. B., & Kiel, B. (2015). Denitrification in the Mississippi River network controlled by flow through river bedforms. *Nature Geoscience*, 8(12), 941–945. https://doi.org/10.1038/ngeo2567
- Hall, R. O., Tank, J. L., Sobota, D. J., Mulholland, P. J., O'Brien, J. M., Dodds, W. K., et al. (2009). Nitrate removal in stream ecosystems measured by 15N addition experiments: Total uptake. *Limnology & Oceanography*, 54(3), 653–665. https://doi.org/10.4319/lo.2009.54.3.0653
- Harvey, J., Gomez-Velez, J., Schmadel, N., Scott, D., Boyer, E., Alexander, R., et al. (2019). How hydrologic connectivity regulates water quality in river corridors. *Journal of the American Water Resources Association*, 55(2), 369–381. https://doi.org/10.1111/1752-1688.12691
- Heffernan, J. B., & Cohen, M. J. (2010). Direct and indirect coupling of primary production and diel nitrate dynamics in a subtropical spring-fed river. Limnology & Oceanography, 55(2), 677–688. https://doi.org/10.4319/lo.2010.55.2.0677
- Heffernan, J. B., Cohen, M. J., Frazer, T. K., Thomas, R. G., Rayfield, T. J., Gulley, J., et al. (2010). Hydrologie and biotic influences on nitrate removal in a subtropical spring-fed river. *Limnology & Oceanography*, 55(1), 249–263. https://doi.org/10.4319/lo.2010.55.1.0249

ZHANG ET AL. 15 of 17



- Helton, A. M., Poole, G. C., Meyer, J. L., Wollheim, W. M., Peterson, B. J., Mulholland, P. J., et al. (2011). Thinking outside the channel: Modeling nitrogen cycling in networked river ecosystems. Frontiers in Ecology and the Environment, 9(4), 229–238. https://doi.org/10.1890/080211
  Hensley, R. T., & Cohen, M. J. (2016). On the emergence of diel solute signals in flowing waters. Water Resources Research, 52(2), 759–772. https://doi.org/10.1002/2015WR017895
- Hensley, R. T., Cohen, M. J., & Korhnak, L. V. (2015). Hydraulic effects on nitrogen removal in a tidal spring-fed river. Water Resources Research, 51(3), 1443–1456. https://doi.org/10.1002/2014WR016178
- Hester, E. T., Brooks, K. E., & Scott, D. T. (2018). Comparing reach scale hyporheic exchange and denitrification induced by instream restoration structures and natural streambed morphology. *Ecological Engineering*, 115, 105–121. https://doi.org/10.1016/j.ecoleng.2018.01.011
- Jarvie, H. P., Sharpley, A. N., Kresse, T., Hays, P. D., Williams, R. J., King, S. M., & Berry, L. G. (2018). Coupling high-frequency stream metabolism and nutrient monitoring to explore biogeochemical controls on downstream nitrate delivery. *Environmental Science and Technology*, 52(23), 13708–13717, https://doi.org/10.1021/acs.est.8b03074
- Julian, J. P., Doyle, M. W., & Stanley, E. H. (2008). Empirical modeling of light availability in rivers. *Journal of Geophysical Research*, 113(3), 3022. https://doi.org/10.1029/2007JG000601
- Junge, F. W., Hanisch, C., Zerling, L., & Gehre, M. (2005). Geochemical signatures (C, N, δ13C, δ15 N, metals) of suspended matter in the river Weiße Elster (central Germany): Their seasonal and flow-related distribution 1997-2001. Isotopes in Environmental and Health Studies, 41(2), 141–159. https://doi.org/10.1080/10256010500131874
- Kamjunke, N., Mages, M., Büttner, O., Marcus, H., & Weitere, M. (2015). Relationship between the elemental composition of stream biofilms and water chemistry—A catchment approach. *Environmental Monitoring and Assessment*, 187(7), 432. https://doi.org/10.1007/s10661-015-4664-6
- Kemp, M. J., & Dodds, W. K. (2002). Comparisons of nitrification and denitrification in prairie and agriculturally influenced streams. *Ecological Applications*, 12(4), 998–1009. https://doi.org/10.1890/1051-0761(2002)012[0998:CONADI]2.0.CO;2
- Kunz, J. V., Hensley, R., Brase, L., Borchardt, D., & Rode, M. (2017). High frequency measurements of reach scale nitrogen uptake in a fourth order river with contrasting hydromorphology and variable water chemistry (Weiße Elster, Germany). Water Resources Research, 53(1), 328–343. https://doi.org/10.1002/2016WR019355
- LHW. (2022). Landesbetrieb für Hochwasserschutz und Wasserwirtschaft Sachsen-Anhalt: Datenportal des Gewässerkundlichen Landesdienstes Sachsen-Anhalt. [Dataset]. Retrieved from https://gld.lhw-sachsen-anhalt.de. accessed 1/19/2023.
- Lupon, A., Martí, E., Sabater, F., & Bernal, S. (2016). Green light: Gross primary production influences seasonal stream N export by controlling fine-scale N dynamics. Ecology, 97(1), 133–144. https://doi.org/10.1890/14-2296.1
- Mulholland, P. J., Hall, R. O., Sobota, D. J., Dodds, W. K., Findlay, S. E. G., Grimm, N. B., et al. (2009). Nitrate removal in stream ecosystems measured by 15N addition experiments: Denitrification. *Limnology & Oceanography*, 54(3), 666–680. https://doi.org/10.4319/lo.2009.54.3.0666
- Mulholland, P. J., Helton, A. M., Poole, G. C., Hall, R. O., Hamilton, S. K., Peterson, B. J., et al. (2008). Stream denitrification across biomes and its response to anthropogenic nitrate loading. *Nature*, 452(7184), 202–205. https://doi.org/10.1038/nature06686
- Mulholland, P. J., Tank, J. L., Webster, J. R., Bowden, W. B., Dodds, W. K., Gregory, S. V., et al. (2002). Can uptake length in streams be determined by nutrient addition experiments? Results from an interbiome comparison study. *Journal of the North American Benthological Society*, 21(4), 544–560. https://doi.org/10.2307/1468429
- Odum, H. T. (1956). Primary production in flowing waters. Limnology & Oceanography, 1(2), 102–117. https://doi.org/10.4319/lo.1956.1.2.0102
  Odum, H. T. (1957). Trophic structure and productivity of silver springs, Florida. Ecological Monographs, 27(1), 55–112. https://doi.org/10.2307/1948571
- Pellerin, B. A., Saraceno, J. F., Shanley, J. B., Sebestyen, S. D., Aiken, G. R., Wollheim, W. M., & Bergamaschi, B. A. (2012). Taking the pulse of snowmelt: In situ sensors reveal seasonal, event and diurnal patterns of nitrate and dissolved organic matter variability in an upland forest stream. *Biogeochemistry*, 108(1–3), 183–198. https://doi.org/10.1007/s10533-011-9589-8
- Reisinger, A. J., Tank, J. L., Hoellein, T. J., & Hall, R. O. (2016). Sediment, water column, and open-channel denitrification in rivers measured using membrane-inlet mass spectrometry. *Journal of Geophysical Research: Biogeosciences*, 121(5), 1258–1274. https://doi.org/10.1002/2015JG003261
- Roberts, B. J., Mulholland, P. J., & Hill, W. R. (2007). Multiple scales of temporal variability in ecosystem metabolism rates: Results from 2 years of continuous monitoring in a forested headwater stream. *Ecosystems*, 10(4), 588–606. https://doi.org/10.1007/s10021-007-9059-2
- Rode, M., Halbedel Née Angelstein, S., Anis, M. R., Borchardt, D., & Weitere, M. (2016). Continuous in-stream assimilatory nitrate uptake from high-frequency sensor measurements. *Environmental Science and Technology*, 50(11), 5685–5694. https://doi.org/10.1021/acs.est.6b00943
- Rode, M., Wade, A. J., Cohen, M. J., Hensley, R. T., Bowes, M. J., Kirchner, J. W., et al. (2016). Sensors in the stream: The high-frequency wave of the present. *Environmental Science and Technology*, 50(19), 10297–10307. https://doi.org/10.1021/acs.est.6b02155
- Smith, V. H. (2003). Eutrophication of freshwater and coastal marine ecosystems: A global problem. *Environmental Science and Pollution Research*, 10(2), 126–139. https://doi.org/10.1065/espr2002.12.142
- Smith, V. H., Tilman, G. D., & Nekola, J. C. (1999). Eutrophication: Impacts of excess nutrient inputs on freshwater, marine, and terrestrial ecosystems. *Environmental Pollution*. 100(1–3), 179–196. https://doi.org/10.1016/S0269-7491(99)00091-3
- Sobota, D. J., Johnson, S. L., Gregory, S. V., & Ashkenas, L. R. (2012). A stable isotope tracer study of the influences of adjacent land use and riparian condition on fates of nitrate in streams. *Ecosystems*, 15(1), 1–17. https://doi.org/10.1007/s10021-011-9489-8
- Sweeney, B. W., Bott, T. L., Jackson, J. K., Kaplan, L. A., Newbold, J. D., Standley, L. J., et al. (2004). Riparian deforestation, stream narrowing, and loss of stream ecosystem services. *Proceedings of the National Academy of Sciences*, 101(39), 14132–14137. https://doi.org/10.1073/pnas.0405895101
- Tank, J. L., Martí, E., Riis, T., von Schiller, D., Reisinger, A. J., Dodds, W. K., et al. (2018). Partitioning assimilatory nitrogen uptake in streams: An analysis of stable isotope tracer additions across continents. *Ecological Monographs*, 88(1), 120–138. https://doi.org/10.1002/ecm.1280
- Tesi, T., Langone, L., Goñi, M. A., Miserocchi, S., & Bertasi, F. (2008). Changes in the composition of organic matter from prodeltaic sediments after a large flood event (Po River, Italy). Geochimica et Cosmochimica Acta, 72(8), 2100–2114. https://doi.org/10.1016/j.gca.2008.02.005
- Tsivoglou, E. C., & Neal, L. A. (1976). Tracer measurement of reaeration: III. Predicting the reaeration capacity of inland streams. *Journal of the Water Pollution Control Federation*, 48(12), 2669–2689. Retrieved from https://www.jstor.org/stable/25040082
- Wagenschein, D., & Rode, M. (2008). Modelling the impact of river morphology on nitrogen retention-A case study of the Weisse Elster River (Germany). Ecological Modelling, 211(1-2), 224-232. https://doi.org/10.1016/j.ecolmodel.2007.09.009
- Welsh, D. T., Bartoli, M., Nizzoli, D., Castaldelli, G., Riou, S. A., & Viaroli, P. (2000). Denitrification, nitrogen fixation, community primary productivity and inorganic-N and oxygen fluxes in an intertidal Zostera noltii meadow. *Marine Ecology Progress Series*, 208, 65–77. https://doi.org/10.3354/meps208065
- Wollschläger, U., Attinger, S., Borchardt, D., Brauns, M., Cuntz, M., Dietrich, P., et al. (2017). The Bode hydrological observatory: A platform for integrated, interdisciplinary hydro-ecological research within the TERENO Harz/central German lowland observatory. *Environmental Earth Sciences*, 76(1), 29. https://doi.org/10.1007/s12665-016-6327-5

ZHANG ET AL. 16 of 17



## **Water Resources Research**

- 10.1029/2022WR032329
- Yang, X., Jomaa, S., Büttner, O., & Rode, M. (2019). Autotrophic nitrate uptake in river networks: A modeling approach using continuous high-frequency data. *Water Research*, 157, 258–268. https://doi.org/10.1016/j.watres.2019.02.059
- Zhang, X., Yang, X., Hensley, R., Lorke, A., & Rode, M. (2022). Quantify instream metabolism and N uptake based on two-station mass balance method. [Dataset]. Helmholtz-Centre for Environmental Research. https://doi.org/10.48758/UFZ.12911
- Zhao, Y., Xia, Y., Ti, C., Shan, J., Li, B., Xia, L., & Yan, X. (2015). Nitrogen removal capacity of the river network in a high nitrogen loading region. *Environmental Science and Technology*, 49(3), 1427–1435. https://doi.org/10.1021/es504316b
- Zheng, L., & Bayani Cardenas, M. (2018). Diel stream temperature effects on nitrogen cycling in hyporheic zones. *Journal of Geophysical Research: Biogeosciences*, 123(9), 2743–2760. https://doi.org/10.1029/2018JG004412

# **References From the Supporting Information**

- Baird, R. B., Eaton, A. D., & Rice, E. W. (Eds.) (2017). Standard methods for the Examination of water and wastewater (23rd ed.). American Public Health Association.
- Guse, B., Bronstert, A., Rode, M., Tetzlaff, B., & Wendland, F. (2007). Application of two phosphorus models with different complexities in a mesoscale river catchment. *Advances in Geosciences*, 11, 77–84. Copernicus GmbH. https://doi.org/10.5194/adgeo-11-77-2007
- Yang, X., Jomaa, S., Zink, M., Fleckenstein, J. H., Borchardt, D., & Rode, M. (2018). A new fully distributed model of nitrate transport and removal at catchment scale. Water Resources Research, 54(8), 5856–5877. https://doi.org/10.1029/2017WR022380
- Zhang, X., Yang, X., Jomaa, S., & Rode, M. (2020). Analyzing impacts of seasonality and landscape gradient on event-scale nitrate-discharge dynamics based on nested high-frequency monitoring. *Journal of Hydrology*, 591, 125585. https://doi.org/10.1016/j.jhydrol.2020.125585

ZHANG ET AL. 17 of 17